Title	Stroboscopic Hamiltonian engineering in the low-frequency regime with a one-dimensional quantum processor
Author(s)	V. M. Bastidas, Haug, C. Gravel, L.-C. Kwek, W. J. Munro, and Kae Nemoto

This is the published version of the following article:

Bastidas, V. M., Haug, T., Gravel, C., Kwek, L.-C., Munro, W. J., & Nemoto, K. (2022). Stroboscopic Hamiltonian engineering in the low-frequency regime with a one-dimensional quantum processor. *Physical Review B, 105*(7), Article 075140. https://doi.org/10.1103/PhysRevB.105.075140

Stroboscopic Hamiltonian engineering in the low-frequency regime with a one-dimensional quantum processor

V. M. Bastidas,[1,2,*] T. Haug,[1,3,*] C. Gravel,[2,†] L.-C. Kwek,[3,4,5] W. J. Munro,[1,2] and Kae Nemoto[2,‡]

[1]*NTT Research Center for Theoretical Quantum Physics, NTT Corporation, 3-1 Morinosato-Wakamiya, Atsugi, Kanagawa, 243-0198, Japan*

[2]*National Institute of Informatics, 2-1-2 Hitotsubashi, Chiyoda-ku, Tokyo 101-8430, Japan*

[3]*Centre for Quantum Technologies, National University of Singapore, 3 Science Drive 2, Singapore 117543, Singapore*

[4]*MajuLab, CNRS-UNS-NUS-NTU International Joint Research Unit, UMI 3654, Singapore 117543, Singapore*

[5]*National Institute of Education, Nanyang Technological University, 1 Nanyang Walk, Singapore 637616, Singapore*

(Received 30 August 2020; revised 17 January 2022; accepted 9 February 2022; published 22 February 2022)

We propose a scheme to perform stroboscopic Hamiltonian engineering in the low frequency regime using a quantum system with one-dimensional nearest-neighbor coupling that are commonly available in the NISQ era. Computational problems are encoded in the effective Hamiltonian of the quantum systems under the effect of external driving. Our approach is nonperturbative and it does not rely on high-frequency expansions, which are a common tool in Floquet engineering. In our paper, the effective Hamiltonian that we want to engineer is fully tailored through designing the periodic driving. We illustrate how this quantum computation proceeds with two examples, an instance from the 3-SAT problem and the LiH molecule quantum chemistry simulation. In the case of the 3-SAT Hamiltonian, we show that by starting from the ground state of the trivial Hamiltonian, the quantum systems go through an adiabatic process in the stroboscopic picture towards the target Hamiltonian of the problem.

DOI: 10.1103/PhysRevB.105.075140

I. INTRODUCTION

Quantum computers are rapidly extending their capability through the enormous efforts around the world [1–4]. The first step to use quantum computers is to encode a problem, which could be a quantum chemistry simulation, in either the unitary process or the Hamiltonian of the quantum computer [5,6]. The unitary processes are given by an appropriate algorithm and then are decomposed into one- and two-qubit gates to be implemented on the quantum computer [7–9]. The gate structure is the natural pathway to achieve scalable fault-tolerant quantum computer [10]. However it is questionable if such machine operation is optimal for quantum systems in the noisy intermediate-scale quantum (NISQ) regime [1,11]. The other approach is to encode the problem we want to solve in the Hamiltonian, which is commonly used in adiabatic quantum computation and its variants [12]. This has its benefits as the control of quantum computer can be simplified [13], which could reduce errors and contribute a longer coherence time of the quantum system [14]. However, the aforementioned approach suffers from the fundamental difficulty to realize arbitrary Hamiltonians [13,15–17]. Currently there have been huge efforts to implement a programmable two-body interaction on a quantum computer or quantum simulator. However, it is well known that hard problems involve more complex many-body interactions [12,18,19] whose practical implementation may require a large resource cost [20,21]. The implementation of those ideas to realize fully programmable two-body interactions and to circumvent the necessity of multi-body interaction with the geometrical constraints from the experimental setup remains challenging.

To overcome the fundamental obstacles of quantum computers in the NISQ regime, we propose a hybrid approach to perform the encodings discussed above. We start with the simplest quantum processors with the capability for individual qubit control; superconducting [22–24] and trapped ions [8,25,26] as ideal platforms to implement our ideas. These devices are highly programmable and can be controlled, enabling the tuning of on-site energies and couplings [4,24,27–29]. We exploit this control capability to modulate in time parameters of the system, which is a simpler task than applying quantum gates. This has already been achieved in diverse platforms ranging from superconducting qubits to ion traps and cold atoms [4,24,27–31].

Now, to combine the advantages from both encoding approaches, we use the system's time-evolution, that is the unitary process, to define the Hamiltonian where we encode the problem to solve. By applying a periodic drive, the system Hamiltonian has the property $\hat{H}(t) = \hat{H}(t+T)$. This means that in the stroboscopic picture, the time evolution over the interval T, $\hat{U}(T;0) = \hat{\mathcal{F}}$, defines an effective Hamiltonian via $\hat{\mathcal{F}} = \exp(-i\hat{H}_{\text{eff}}T/\hbar)$. Here $\hat{\mathcal{F}}$ is the Floquet operator for this periodically driven system [32–36]. We illustrate in Fig. 1 the basic concept of the physical system and the periodic drive which is discretized for the numerical optimization described later in this paper.

*These authors contributed equally to this work.

†Present address: EAGLYS, #301 Utsumi Building, 1-55-14 Yoyogi, Shibuya-ku, Tokyo, 151-0053, Japan.

‡nemoto@nii.ac.jp

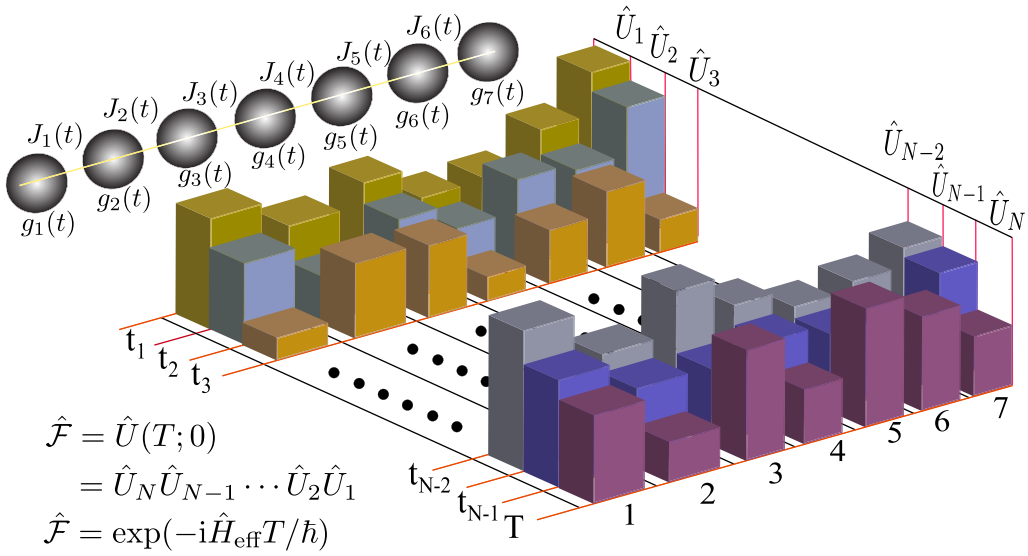

FIG. 1. Schematic illustration of a one-dimensional qubit array driven individually by external pulses. The graph details how the parameter control can be designed for the Floquet operator.

The form of the effective Hamiltonian $\hat{H}_{\text{eff}}$ is determined by the driving sequence, which can be exploited to perform Floquet engineering based on perturbative high-frequency expansions [33–37]. This is a powerful approach that has proven to be useful to enable the implementation of quantum computation by applying local control to spin chains [38,39]. In nuclear magnetic resonance (NMR), the effect of periodic pulses has proven to be extremely effective to suppress the noise due to coupling to an external environment [40]. In NMR the periodic pulses can also be used to simulate effective Hamiltonians by using the average Hamiltonian theory (AHT) [40,41], which in practice is the same as Floquet engineering. To apply AHT, however, one has to work in the high-frequency regime [42].

In our paper, we focus on a different approach to tackle the problem of Hamiltonian engineering. The conventional wisdom is that the low-frequency regime is useless for quantum simulation as the system heats up and reach an infinite-temperature state in the long-time limit [29,32,43]. In contrast to the usual approach to Floquet engineering, we propose how to exploit the low-frequency regime in a nonperturbative fashion to engineer our desired effective Hamiltonian at stroboscopic times. We consider a situation where the couplings between the qubits and their on-site energies can be modulated in time. For example, we can keep the couplings on during the evolution thus resembling analog simulators, while applying local rotations to the qubits that are operations used in digital quantum simulators. Alternatively, we can also modulate the couplings and the on-site energies. Here is important to note that in contrast to previous papers, the control sequences are obtained through an optimization algorithm and not by resorting to Suzuki-trotter decompositions of the target Hamiltonian that we aim to generate. In fact, there has been an enormous interest on digital-analog quantum computers [44–46] and digital-analog quantum simulators [47,48], where one can exploit the best features of analog and digital devices.

By using optimization tools, we find a nearly optimal periodic control that allows us to generate an effective Hamiltonian arbitrarily close to the Hamiltonian of the problem that we want to solve. Similar ideas have been proposed to engineer couplings between superconducting qubits [49] and in a recent experimental demonstration in cold atoms [50]. Our approach is fundamentally different to previous approaches to quantum control using GRAPE, where the goal is to find an optimal control sequence to reach a target state, which is relevant for nuclear magnetic resonance (NMR) [51–55]. A recent experiment demonstrates that a 12-qubit system can be employed as a quantum processor to optimize its own control sequence by using measurement-based feedback control (MQFC), which can avoid the use of GRAPE to optimize control sequences in order to achieve a target state [56].

The essential element of Floquet engineering is not the periodicity of the drive, but the interpretation of the dynamics in terms of the effective Hamiltonian [57,58]. In this paper, we advance this approach to propose a fully-programmable technique in a one-dimensional qubit array to engineer arbitrary effective Hamiltonians using the low frequency regime. We use the effective Hamiltonian to carry all the data of the target Hamiltonian matrix in a chosen basis. Before going into the details about how it can be done, let us first describe the physical system of our NISQ computer.

II. MODEL

We have several choices of the physical system, and the properties of the quantum computer are dependent on the implementation model [1]. For instance, superconducting-qubit-based NISQ devices in an L qubit one-dimensional

array with nearest-neighbors coupling can be described by [22,24,28,29]

$$\hat{H}(t) = \hbar \sum_{l=1}^{L} \left[g_l(t)\hat{n}_l + \frac{U}{2}\hat{n}_l(\hat{n}_l - 1) \right] + \hbar \sum_{l=1}^{L-1} J_l(t)\left[\hat{a}_l^\dagger \hat{a}_{l+1} + \hat{a}_l \hat{a}_{l+1}^\dagger\right], \quad (1)$$

where $\hat{n}_l = \hat{a}_l^\dagger \hat{a}_l$ is the number operator with $\hat{a}_l$ and $\hat{a}_l^\dagger$ being the bosonic annihilation and creation operators at site l, respectively. In superconducting qubit arrays, the bosonic excitations are microwave photons. Now with current experimental feasibilities, Z and XY control lines of the superconducting processor can be used to drive the angular frequencies of the qubits $g_l(t)$ and the coupling strengths $J_l(t)$, whereas the anharmonicity U is kept fixed and determined from fabrication. The model in (1) is not restricted to superconducting circuit and is equally valid for 1D arrays in cold atoms [31].

Now in the regime $U \gg g_l, J_l$ (the hardcore boson regime where the large anharmonicity prevents two excitations from being at the same site [4,24]), Eq. (1) can be rewritten in a qubit form where the system Hamiltonian is given in terms of the usual Pauli operators σ_l^α with $\alpha \in \{x, y, z\}$ as

$$\hat{H}(t) = \frac{\hbar}{2} \sum_{l=1}^{L} g_l(t)\sigma_l^z + \frac{\hbar}{2} \sum_{l=1}^{L-1} J_l(t)\left(\sigma_l^x \sigma_{l+1}^x + \sigma_l^y \sigma_{l+1}^y\right). \quad (2)$$

This model is also suitable for implementations with quantum dots [59] and lattice defects [60,61] for instance. When the number of excitation M is one, both Hamiltonians (1) and (2) are the same. The number of excitations are conserved in both models, and the dimension of the Hilbert space is L for $M = 1$, which is significantly smaller than 2^L. The dimension of the Hilbert space gives the upper limit for the computational size, such that an $L \times L$ Hermitian matrix can be implemented for $M = 1$. If the model allows us to implement arbitrary unitaries up to this dimension, the system is a universal quantum computer. This can be confirmed by algebraic properties of Hamiltonian (2) written in terms of SU(L) operators. At this stage we want to emphasis our approach while able to engineer any effective Hamiltonian is not scalable. It can solve any problem that fits within the size of the computational space that can be realized.

Next when we move to multiple excitations ($M > 1$) these models given in (1) and (2) behave differently. Consider the model given by Hamiltonian (1), where the computational basis for this model differs from the basis used for the qubit-based quantum computer. Here we have states with two excitations in one site as well as others, although the population of these states may be small when U is large. Thus, the model described by Hamiltonian (1) has a Hilbert space whose dimension now depends on the number of excitations $M > 1$. In the absence of interactions ($U = 0$), we have already observed the usefulness of the expansion of the Hilbert space with increasing the number of excitations in boson sampling [62,63]. Though unlike boson sampling, this model is universal when we include interactions with strength U [64]. We also would like to add that in the context of analog devices, it has been shown that it is possible to use a one-dimensional quantum system with 9 states per particle to perform universal quantum computation [18].

In the case of the Hamiltonian (2) for hardcore bosons, the dimension of the computational space is restricted to a subspace of the 2^L-dimensional Hilbert space. Further, the system dimension is smaller than in the bosonic case with finite U, where the dimension is ${}^{L+M-1}C_M$. Thus, by using the same M, one can extend the computational space. We note that in the hardcore boson limit with $M > 1$ quantum computation is not universal, as the system dynamics is constrained by symmetries. In contrast, in the case of Hamiltonian (1) for finite U, the system's dynamics is universal for SU(${}^{L+M-1}C_M$) and any M. After discussing the controllability of physical system we are interested in, next let us briefly discuss the numerical technique used to find the driving sequences used to engineer the target Hamiltonian.

III. OPTIMIZATION OF DRIVING SEQUENCES USING GRAPE

The first step in the optimization of the driving sequence is to set the Hamiltonian $\hat{H}_{\text{trial}}$ as the effective Hamiltonian with a trial driving sequence, and then optimize the trial driving sequence to be the one that gives the target Hamiltonian $\hat{H}_{\text{target}}$. The trial Hamiltonian $\hat{H}_{\text{trial}}$ can be evaluated by the fidelity between $\hat{H}_{\text{trial}}$ and $\hat{H}_{\text{target}}$ as $F = |\text{tr}(\hat{\mathcal{F}}_{\text{target}}^\dagger \hat{\mathcal{F}}_{\text{trial}})|/D$, where D is the dimension of the Hilbert space and F can take values between 0 and 1 being reached when the $\hat{\mathcal{F}}_{\text{trial}}$ is equal to $\hat{\mathcal{F}}_{\text{target}}$. The trial Hamiltonian $\hat{H}_{\text{trial}}$ can be optimized via GRAPE [65–67]. As we mentioned before, the driving sequences are discretized for the numerical optimization as $\hat{\mathcal{F}} = \hat{U}(T;0) = \hat{U}_N \hat{U}_{N-1} \cdots \hat{U}_2 \hat{U}_1$ at different time steps $t_j = j\tau$ with $\tau = T/N$. The propagator of the jth time step $t_j = j\tau$ is given as $\hat{U}_j = e^{-i\hat{H}_u(t_j)\tau/\hbar}$ with the total Hamiltonian for time step t_j as $\hat{H}_u(t_j) = \hat{H}_d + \sum_{k=1}^{R} u_k(t_j)\hat{V}_k$ where $\hat{H}_d$ is a constant drift Hamiltonian term $\hat{H}_d$. Next the R hermitian control operators $\hat{V}_j$ depend on the scalar control function $u_j(t)$ and are initially chosen at random, and are to be optimized to achieve the desired target unitary $\hat{\mathcal{F}}_{\text{target}}$.

The method of choice here is gradient descent using L-BFGS-B (bounded, limited memory Broyden-Fletcher-Goldfarb-Shanno algorithm) within the Qutip implementation [66], where we optimize the fidelity by taking small steps in the control parameters by following the gradient of the fidelity. The gradients $\partial F(\hat{U}_j)/\partial u_k(t_j)$ can be calculated by invoking the spectral theorem [65], and then all the control parameters are updated at the same time. This procedure is repeated until convergence. As gradient descent is known to become stuck in local minima [68], we ran the algorithm 5 times, starting from random initial driving protocols. For each run, fidelity is optimized for maximally 10 000 runs or the magnitude of the gradient for the optimization becomes smaller than 10^{-10}, whichever is satisfied first. Then, we choose the maximum fidelity of all 5 runs. Normally, we find that at least 3 of the 5 runs converge to the same maximal value of fidelity. We have made our numerical code available in Github [69].

A next step after discussing the optimization algorithm is to analyze the type of Hamiltonians that can be simulated in

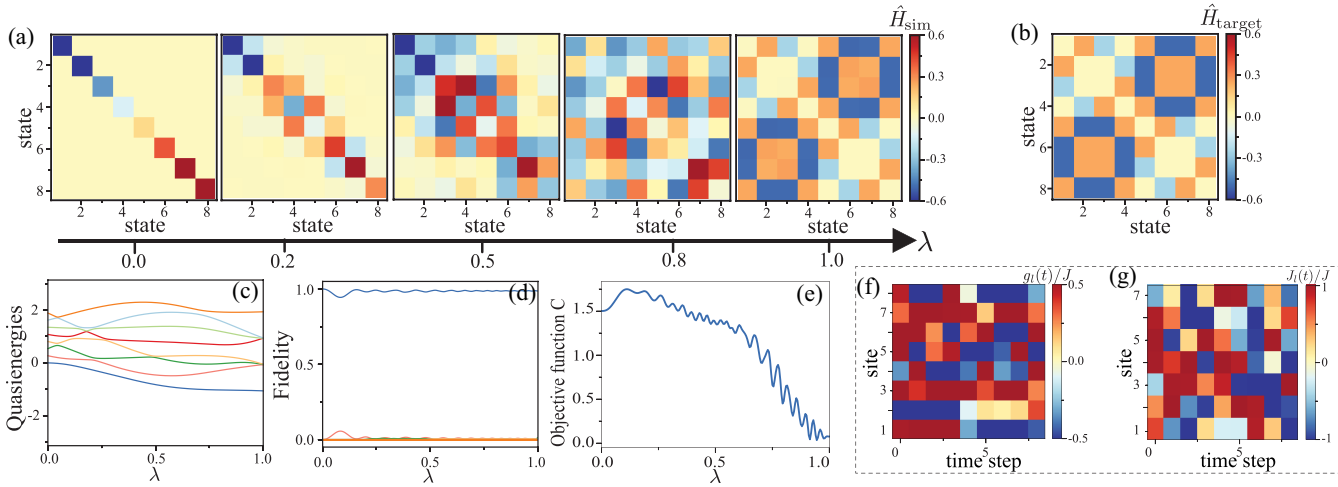

FIG. 2. Hamiltonian engineering for a 3-SAT problem with three-body interactions and adiabatic deformation between effective Hamiltonians. (a) Shows the adiabatic process from the initial Hamiltonian to the final Hamiltonian. (b) Represents the Hamiltonian of the 3-SAT problem in the matrix form. (c) Shows the quasienergies as a function of λ. (d) Illustrates the fidelity between the state of system and instantaneous eigenstates of effective Hamiltonian. The adiabatic evolution occurs over a total time of $T_{\rm total} = 200T = 1276/J$, where $T = 6.38/J$ is the period of the drive. In (e) we depict the expectation value of the cost function $\hat{C} = \frac{1}{4}(\mu_1^x - \mu_2^x + \mu_3^x - 2\mu_1^x\mu_2^x - 2\mu_1^x\mu_3^x + \mu_1^x\mu_2^x\mu_3^x)$ in the instantaneous ground state of the effective Hamiltonian. [(f),(g)] Are the required driving sequences.

certain parameter regimes of the device. We will now illustrate how the quantum computational process take place with two examples that show the versatility of our approach in diverse areas such as combinatorial optimization and quantum chemistry.

IV. HAMILTONIAN ENGINEERING AND ADIABATIC DEFORMATION: A MINIMAL EXAMPLE OF 3-SAT SOLVER

The first example is an instance of 3-SAT solver for combinatorial optimization. The term SAT itself refers to satisfiability of equations involving boolean variables and some variants of SAT problems are hard [70]. 3-SAT problems are of utmost importance because any k-SAT problem can be decomposed into a sequence of 3-SAT instances. Our instance is a 3-SAT problem to solve the clauses

$$a_2 + a_3 + a_1a_3 = 1,$$
$$a_1 + a_3 + a_1a_2 = 1,$$
$$a_1 + a_2 + a_2a_3 = 0,$$

where a_1, a_2, and a_3 are boolean variables. It is straightforward to map [71] this combinatorial problem to a spin Hamiltonian of the form

$$\hat{H}_{\rm SAT} = \hbar\omega\left(\mu_1^x - \mu_2^x + \mu_3^x - 2\mu_1^x\mu_2^x - 2\mu_1^x\mu_3^x + \mu_1^x\mu_2^x\mu_3^x\right), \tag{3}$$

where μ_l^α are Pauli matrices with ω a scaling parameter see Appendix C. The simplest 3-SAT problems involve 3-body interactions [70], which is usually problematic to implement, however with our approach, we only need to map the matrix data [see Fig. 2(b)] to the effective Hamiltonian which is not an obstacle.

The goal of this quantum computation is to find its ground state, corresponding to the triplet (a_1, a_2, a_3) satisfying the 3 clauses discussed above. In the eigenbasis of μ_l^z, the matrix representation of the target Hamiltonian (C10) is a 8×8 matrix [depicted in Fig. 2(b)]. Now to map this target Hamiltonian to the effective Hamiltonian we can use a single-excitation and Hamiltonians (1) or (2). Once we have found the driving sequences shown in Figs. 2(f) and 2(g) for the on-site energy g_l and the coupling parameter J_l respectively, we set the effective Hamiltonian to be the final Hamiltonian in the adiabatic passage in the stroboscopic picture [72]. We begin with an initialized state, which is the ground state of a trivial Hamiltonian, then the system goes through an adiabatic transformation at the times nT by gradually changing the control sequence, forming an adiabatic passage in the stroboscopic picture [72]. Figure 2(a) illustrates the stroboscopic adiabatic process for this instance. The initial state is the ground state of the local Hamiltonian and then the driving sequences for g_l and J_l are gradually changed to the sequences shown in (f) and (g) as the stroboscopic time $\lambda \to 1$. At $\lambda = 1$ the adiabatic transformation is completed, and the system is at the ground state of the final Hamiltonian [the right plot in (a)] with a high probability. We note that the intermediate Hamiltonian $\hat{H}_{\rm eff}(\lambda)$ is not restricted to the sum of the initial and final Hamiltonians [73]. To speed up the computational time, methods used in quantum annealing such as avoiding phase transitions could be applied [74], and such freedom of the pathway could be exploited, however we leave this for future.

To illustrate the behavior of our approach we show the quasi-eigenenergies exhibiting multiple anticrossings in Fig. 2(c) and fidelity for our system remaining in the ground state in Fig. 2(d). Our results indicate that the system remains the lowest quasi-eigenenergy state with the high fidelity implying the high success probability of the computation. Reading out this output state, we obtain the solution $(a_1, a_2, a_3) = (0, 0, 1)$ satisfying the three clauses discussed above. It is useful to give the details of how the driving

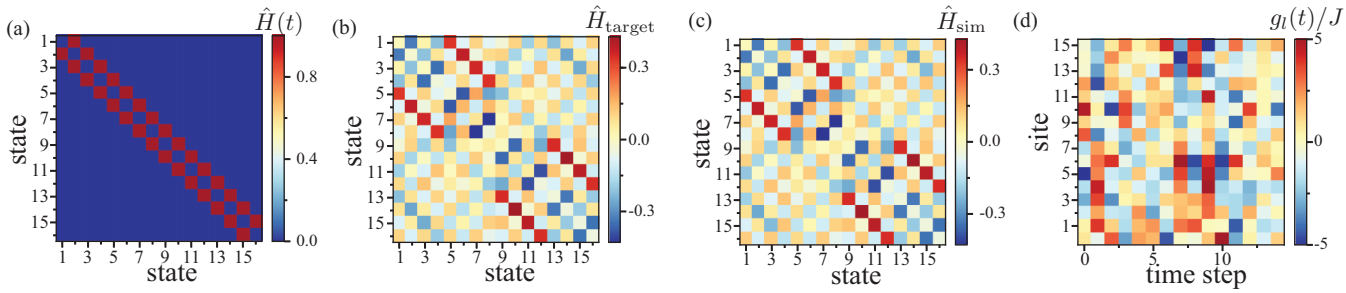

FIG. 3. Simulation of LiH with Floquet engineering where the molecule is mapped to a 16 dimensional Hilbert space. (a) Depicts the instantaneous nearest-neighbor Hamiltonian of a linear chain with $L = 16$ sites and one excitation ($M = 1$). (b) Shows the target Hamiltonian, while (c) depicts the effective Hamiltonian generated by driving local potential of linear chain. d) Illustrates the driving sequence $-5J < g_l < 5J$ applied to generate the effective Hamiltonian.

sequences for the on-site energy g_l and the coupling parameter J_l in Figs. 2(f) and 2(g) can be obtained.

V. HAMILTONIAN ENGINEERING IN QUANTUM CHEMISTRY: STROBOSCOPIC SIMULATION OF THE LiH MOLECULE

Our approach can of course be used for different problems and so let us now apply it to one in quantum chemistry. Understanding biological processes and designing new pharmaceutical products is of utmost importance in today's age. To accomplish task, we have to understand the inner workings of atoms, molecules and proteins better by calculating their properties such as their quantum mechanical configuration and dynamics from first principles. Quantum computers offer the promise to be able to calculate these properties for large molecules. As benchmark, small molecules can be calculated already with state-of-the-art quantum computers [3]. The Hamiltonian that describes the molecule involves many controlled interactions that involve several qubits. Most quantum computers support only two-body interactions and thus require multiple operations just to fulfill a single operation that involves multiple qubits. With Floquet engineering, all those interactions including the complex k-body (with $k > 1$) terms can directly encoded into the effective Hamiltonian.

We simulate a LiH molecule at the bond distance, where nontrivial many-body terms can be directly encoded into the effective Hamiltonian. The corresponding parameters of the Hamiltonian can be found in [3], where they have been obtained by the STO-3G basis. It approximates the atomic orbitals with three Gaussians to obtain the one and two-electron integrals for the electron interactions [Slater-type orbital (STO)]. For the LiH molecule, the 1s orbital of H and the 1s, 2s and $2p_x$ and $2p_z$ were assumed to be occupied, all other orbitals are assumed to be empty. By including the parity symmetries, the LiH molecule can be described effectively by 4 qubits or a Hilbert space of dimension 16. It consists of 99 coupling terms expressed as a product of different Pauli operators, as we show in Appendix E. Figure 3(b) illustrates the effective Hamiltonian optimized to the target Hamiltonian, whereas (a) shows the instantaneous Hamiltonian of the device. We use a one-dimensional chain with a single excitation $M = 1$ in $L = 16$ sites. In Fig. 3 we can observe the effective Hamiltonian [Fig. 3(b)] has a high fidelity to the target Hamiltonian [Fig. 3(c)]. The driving sequence for the on-site energies g_l is depicted in Fig. 3(d). We perform the simulation following the same method used for the 3-SAT Hamiltonian and the fidelity reached was $F = 0.99954$.

VI. SIMULATING QUANTUM GRAPHS

Finally, we give an estimation for the cost to obtain the effective Hamiltonian in terms of the fidelity and the scaling of the minimal driving period T_{min} to engineer a desired connectivity. First we need to acknowledge that multiple periods will be needed and so these approach could be slow in nature to perform. For this evaluation, we employ star and all-to-all graphs as the target Hamiltonian and begin by evaluating the number of steps N for the discretized Floquet operator. Although a larger N guarantees a high fidelity, the optimization with a larger N costs us a longer time to compute. To estimate the fidelity of the effective Hamiltonian in the single excitation case $M = 1$, in Fig. 4 we plot the fidelity against the driving time T for several different Ns for a star graph with $L = 9$ sites in and all-to-all connected graph with $L = 8$ sites. Figure 4(a) shows the fidelity change as T increasing for driving of the local on-site energy for the star graph and of both the local on-site energy and the coupling parameter for the all-to-all connected graph. We can see the fidelity saturates with relatively small Ns and a comparable time scale to the coupling parameter J.

Lastly, we test the scaling of the optimization as a function of the system size L for different Ms, which is shown in Fig. 4(b) for star and all-to-all connected graphs. In this estimation we use the Hamiltonian (2) in the hardcore boson regime to first calculate the near optimal driving parameters for $M = 1$. The same driving sequence can be then used for the cases $M > 1$. Notably, as depicted Fig. 4(b) one can see that for both connectivities, the scaling of the minimum driving time T_{min} is linear with the number of sites L for different number of particles and driving amplitudes of the on-site energies. Keeping this in mind we decided to investigate the performance of our approach to simulate a device with all-to-all connectivity for different number of excitations $M = 1, 2, 3, 4$ in $L = 8$ sites as depicted in Fig. 5. In this plot, we consider a driving of the on-site energies $-5J < g_l < 5J$ with period $T = 10/J$, and $N = 10$ time steps with a step size

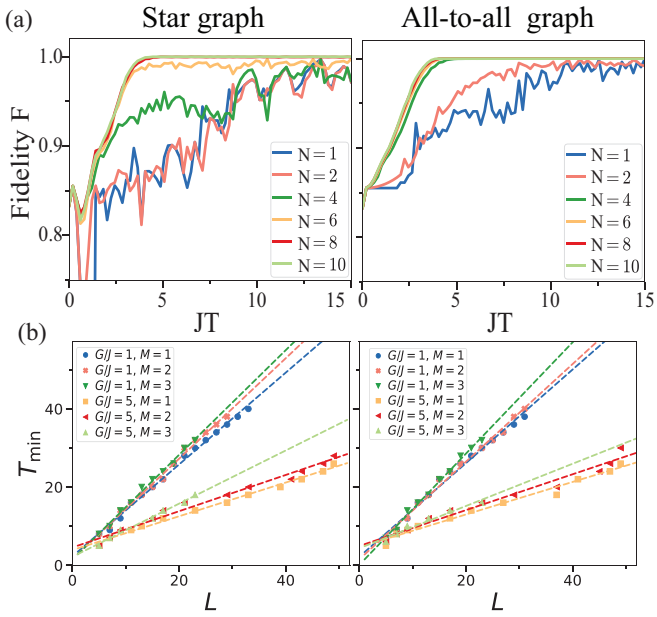

FIG. 4. Dependence of the driving sequence as a function of the parameters. (a) Shows the fidelity as a function of the period T and time steps N for a single excitation $M = 1$ used to generate a star graph with $L = 9$ (by driving local potential $-5J < g_l < 5J$) and an all-to-all connected lattice with $L = 8$ (by driving the local potential g_l and the couplings $-J < J_l < J$). (b) By fixing the step to be $\tau = 1/J$, we calculate the minimal driving period $T_{\min}$ needed to generate an effective Hamiltonian with fidelity $F > 0.999$ for varying system size L and for different driving amplitudes G of the on-site energies $-G \leqslant g_l \leqslant G$ in the case of different number of excitations $M = 1, 2, 3$. The left and right panels illustrate the results for star and all-to-all connected graphs, respectively.

$\tau = 1/J$. In Appendix D we explore the stability of the driving protocol under time dependent noise.

VII. COMPUTATIONAL COST OF OUR APPROACH

In the previous section, we discussed about the scaling of minimal driving period $T_{\min}$ as a function of the number of sites L and its dependence on other parameters of the system. This minimum period is related to the time we need to let the quantum system evolve and it is important for practical applications as the existing devices are affected by errors that accumulate over time. The focus of our paper is to show how to simulate modest-scale interesting systems and the computational cost of the classical algorithm used to find the driving section also plays an important role. Thanks to the conservation of the number of excitations, the Hamiltonian (2) can be decomposed into different subspaces with a fixed number $M = 1, 2...$ of excitations. The size of the Hamiltonian matrix within each subspace increases as we increase M, which in principle, makes the optimization harder. However, we found that if we find a solution for $M = 1$ excitation, we can use this solution to treat problems with higher number of excitations. For this reason, we focus on the computational cost of optimizing the driving sequence in the single-excitation subspace. Figure 6 shows the computational cost to simulate all-to-all connectivity of a device using a single excitation in L sites when the system is in the hardcore boson regime. There one can see that the iterations scale as $\propto L^2$ and the computational time as $T_{\text{comp}} \propto L^{4.2}$ for a driving amplitude $G/J = 5$. This is precisely the driving amplitude used to obtain the results depicted in Fig. 5 for a lattice with $L = 8$ sites.

VIII. CONCLUSIONS

In this paper we have demonstrated how a one-dimensional quantum system with nearest-neighbors couplings can be used to engineer arbitrary Hamiltonians on a NISQ computer. We illustrated how the computation works through two examples from NP complete problems and quantum chemistry simulation. The encoding of the problem to the effective Hamiltonian is done via the operator matrix representation, and hence the approach does not detect any differences to implement many-body interaction for hard problems. We also estimate the encoding cost for various parameters, and our works indicates the validity of this approach for hard problems in the NISQ regime. The computational space of this approach can be easily extended by adding more excitations to the system, without the need to change the device. However as with all NISQ processors there will be a limit which will affect its scalability.

ACKNOWLEDGMENTS

We thank M. P. Estarellas, A. Sakurai, and L. Wright for valuable discussions. This work was supported in part by the Japanese MEXT Quantum Leap Flagship Program (MEXT Q-LEAP), Grant No. JP-MXS0118069605, the MEXT KAKENHI Grant-in-Aid for Scientific Research on Innovative Areas Science of hybrid quantum systems Grant No. 15H05870 and the JSPS KAKENHI Grant No. 19H00662. The computational work for this article was partially performed on resources of the National Supercomputing Centre, Singapore.

APPENDIX A: FLOQUET THEORY AND STROBOSCOPIC DYNAMICS

In our paper we focus on time periodic Hamiltonians $\hat{H}(t + T) = \hat{H}(t)$ where T is the drive period. Due to the periodicity of the Hamiltonian, the most relevant information is contained in the Floquet operator $\hat{\mathcal{F}} = \hat{U}(T; 0) = \hat{\mathcal{T}} \exp[-i/\hbar \int_0^T \hat{H}(s)ds]$, which is the evolution operator within one period of the drive. In the previous equation, we need to use the time-ordering operator $\hat{\mathcal{T}}$. By solving the eigenvalue problem $\hat{\mathcal{F}}|\Phi_\alpha\rangle = e^{-i\varepsilon_\alpha T/\hbar}\Phi_\alpha\rangle$, one can obtain the most relevant information for the dynamics. The eigenvectors $|\Phi_\alpha\rangle$ are known as the Floquet states and $-\hbar\pi/T \leqslant \varepsilon_\alpha \leqslant \hbar\pi/T$ are the quasienergies. As the Floquet operator is unitary, it is possible to define an effective Hamiltonian $\hat{H}_{\text{target}}$ such that $\hat{\mathcal{F}} = \exp(-i\hat{H}_{\text{target}}T/\hbar)$. At stroboscopic times $t_n = nT$ the effective Hamiltonian is the generator of the dynamics. To be more concrete, given an initial state $|\psi(0)\rangle$, its time evolution at times $t_n = nT$ is given by $|\psi(nT)\rangle = \hat{\mathcal{F}}^n|\psi(0)\rangle = \exp(-i\hat{H}_{\text{target}}nT/\hbar)|\psi(0)\rangle$, which looks exactly as the evolution under a time independent Hamiltonian.

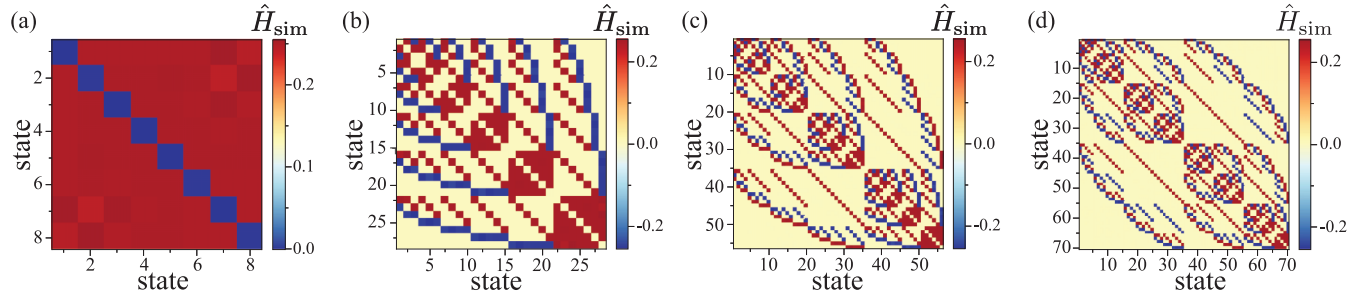

FIG. 5. Matrix representation of the effective Hamiltonian for a device with all-to-all connectivity. In this figure we depict the matrix representation for (a) $M = 1$, (b) $M = 2$, (c) $M = 3$, and (d) $M = 4$ excitations in the hardcore boson regime with driving period $T = 10/J$ and $N = 10$.

APPENDIX B: HARDCORE BOSONS AND THE JORDAN-WIGNER TRANSFORMATION

In this section, we discuss in detail the family of target Hamiltonians that can be simulated using the Hamiltonian

$$\hat{H}(t) = \frac{\hbar}{2}\sum_{l=1}^{L} g_l(t)\sigma_l^z + \frac{\hbar}{2}\sum_{l=1}^{L-1} J_l(t)\left(\sigma_l^x\sigma_{l+1}^x + \sigma_l^y\sigma_{l+1}^y\right) \tag{B1}$$

by describing microwave photons in the hardcore boson regime $U \gg g_l, J_l$. In this case, one can use the Jordan-Wigner transformation [75]

$$\sigma_l^x = f_l^\dagger e^{i\hat{\Phi}_l} + f_l e^{-i\hat{\Phi}_l},$$
$$\sigma_l^y = -if_l^\dagger e^{i\hat{\Phi}_l} + if_l e^{-i\hat{\Phi}_l}, \quad \sigma_l^z = 2f_l^\dagger f_l - 1, \tag{B2}$$

with $\hat{\Phi}_l = \sum_{j<l} f_j^\dagger f_j$ to map the spin Hamiltonian to the fermionic representation

$$\hat{H}(t) = \hbar\sum_{l=1}^{L}[g_l(t)f_l^\dagger f_l + J_l(t)(f_l^\dagger f_{l+1} + \text{H.c.})], \tag{B3}$$

where $f_j^\dagger$ (f_j) are fermionic creation (annihilation) operators. The fermionic representation is versatile, because it gives us a canonical form of the target Hamiltonians that can be achieved by applying a periodic drive

$$\hat{H}_{\rm target} = \hbar\sum_{l=1}^{L}[G_l f_l^\dagger f_l + K_{l,m}(f_l^\dagger f_m + \text{H.c.})]. \tag{B4}$$

Crucially, the effective Hamiltonian allows for long-range hopping of Jordan-Wigner fermions. Due to the nonlocal character of the Jordan Wigner transformation, these long-range hopping become highly nonlocal terms in the spin representation, as follows:

$$\hat{H}_{\rm target} = \frac{\hbar}{2}\sum_{l=1}^{L} G_l\sigma_l^z + \frac{\hbar}{2}\sum_{l,m=1}^{L} K_{l,m}\left(\sigma_l^x\hat{O}_{l,m}\sigma_m^x + \sigma_l^y\hat{O}_{l,m}\sigma_m^y\right), \tag{B5}$$

where $\hat{O}_{l,m} = \sigma_{l+1}^z\sigma_{l+2}^z\cdots\sigma_{m-2}^z\sigma_{m-1}^z$. To simulate a ring, as we discussed in the main text, we require effective couplings between nearest neighbors $K_{l,l+1}$ and to have a coupling $K_{1,L}$. In terms of the spin representation, this leads to an effective Hamiltonian

$$\hat{H}_{\rm target} = \frac{\hbar}{2}\sum_{l=1}^{L} G_l\sigma_l^z + \frac{\hbar}{2}\sum_{l=1}^{L-1} K_{l,l+1}\left(\sigma_l^x\sigma_{l+1}^x + \sigma_l^y\sigma_{l+1}^y\right) + K_{1,L}\left(\sigma_1^x\hat{O}_{1,L}\sigma_L^x + \sigma_1^y\hat{O}_{1,L}\sigma_L^y\right). \tag{B6}$$

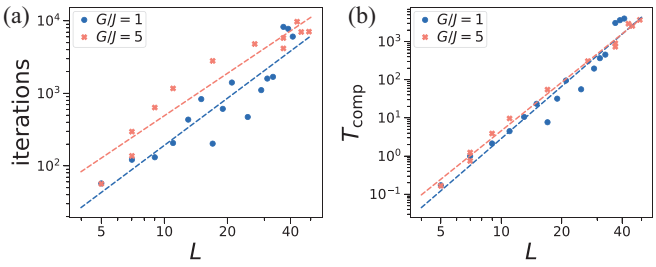

FIG. 6. Computational cost to simulate all-to-all connectivity with a single excitation. (a) Shows the scaling of the number of iterations to achieve convergence of the optimization algorithm without prior knowledge and (b) depicts scaling of the computation time. In both graphs we fix the time step to be $\tau = 1/J$ and show the scaling as a function of the number of sites L for two different driving amplitudes G of the on-site energies $-G \leqslant g_l \leqslant G$. Here, the computational cost is for reaching a fidelity of $F > 0.999$, where the number of bins is chosen such that this fidelity can be reached.

APPENDIX C: A MINIMAL EXAMPLE OF A 3SAT PROBLEM AND ITS ADIABATIC DEFORMATION

In this section, we explain the basic elements on 3SAT problems and its algebraic origin. Let us begin by considering the system of equations given in the main text

$$1 = a_2 + a_3 + a_1a_3, \tag{C1}$$

$$1 = a_1 + a_3 + a_1a_2, \tag{C2}$$

$$0 = a_1 + a_2 + a_2a_3. \tag{C3}$$

For each Eq. (C1), (C2), and (C3) there is an objective function that indicates if an assignment of (a_1, a_2, a_3) satisfies the corresponding equation. We sum up the three objective functions into one that counts the number of solutions for the

entire system. To find an objective function (not necessarily unique), a simple recipe is to use the inclusion-and-exclusion principle. Let C_1, C_2, and C_3 denote respectively objective functions for Eqs. (C1), (C2), and (C3). Then we have

$$C_1 = 1 - (a_2 + a_3 + a_3a_1 - 2(a_2a_3 + a_1a_3 + a_1a_2a_3) + 4a_1a_2a_3), \tag{C4}$$

$$C_2 = 1 - (a_1 + a_3 + a_1a_2 - 2(a_1a_3 + a_1a_2 + a_1a_2a_3) + 4a_1a_2a_3), \tag{C5}$$

$$C_3 = a_1 + a_2 + a_2a_3 - 2(a_1a_2 + a_2a_3 + a_1a_2a_3) + 4a_1a_2a_3. \tag{C6}$$

We sum the former relations and then obtain the following objective function for the entire system:

$$C = 2 - 2a_3 + 3a_1a_3 + a_2a_3 - a_1a_2 - 2a_1a_2a_3. \tag{C7}$$

Let us check that our objective function is right. To do this we construct the table

a_1	a_2	a_3	C
0	0	0	2
0	0	1	0
0	1	0	2
0	1	1	1
1	0	0	2
1	0	1	3
1	1	0	1
1	1	1	1

As the original system represents a permutation, the values of C must follow those of the binomial coefficients $\binom{3}{i}$ for $0 \leqslant i \leqslant 3$. This is not a coincidence and can be easily seen from the inclusion-and-exclusion principle. In a similar way than in adiabatic computation, the initial Hamiltonian is usually tailored such that the algebraic multiplicities of its eigenvalues follow those of the binomial coefficient. We want to point out that Eqs. (C1), (C2), and (C3) are over $\mathbb{Z}_2$ which involve addition and multiplication modulo 2. Some readers might be acquainted with SAT problems involving `true` or `false` together with logical operations of conjunction (and), disjunction (or) and negation (not). There is a one-to-one correspondence between expressions over $\mathbb{Z}_2$ and expressions over {`true`, `false`} involving operations and, or and not. For instance the two simplest nontrivial *irreducible* expressions that lead to 3-SAT problems containing 3 variables are given by

$$x + yz \quad \text{and} \quad x + y + z.$$

We observe that

$$\begin{aligned} x + yz &\Leftrightarrow (x \wedge \neg(y \wedge z)) \vee (\neg x \wedge (y \wedge z)) \\ &\Leftrightarrow (x \wedge (\neg y)) \vee (x \wedge (\neg z)) \vee ((\neg x) \wedge y \wedge z). \end{aligned}$$

Similarly, we can find a logical 3SAT expression for the algebraic 3SAT expression $x + y + z$.

In our example involving Eqs. (C1), (C2), and (C3), there is no point to rewrite the expression into their logical flavor. This is because it is straightforward to obtain the objective function directly from the algebraic 3SAT as we show. Also since there are efficient classical algorithms to solve linear systems of equations over any algebraic field (and even extremely efficient ones over $\mathbb{Z}_2$), there is no point to solve such system with quantum devices. Therefore this explains why we look upon 3-variable systems that are quadratic such as the one obtained from a Toffoli permutation or such as the more cryptographic one given by Eqs. (C1), (C2), and (C3).

The example given by Eqs. (C1), (C2), and (C3) (below in this Appendix Sec. 3) is a typical (toy) example of a system of equations that arises when performing cryptanalysis of block ciphers or hash functions. The algebraic degree of every equation is 2 m, which is high with respect to the maximum possible degree that is 3. The number of terms per equation is high with respect to the maximal number of possible terms which is 8 in our case. Expressed differently and in an equivalent way, the density for the number of terms is relatively high. For more information on properties that matter to system of equations from cryptography, see [76] and [71]. There are 8 possible assignments to the system of equations. The solution space of the system of equations is mapped to the minimal value of the objective function.

1. Obtaining Hamiltonians from cost functions to solve 3SAT instances

Let us recall the objective function from (C7), which is

$$C = 2 - 2a_3 + 3a_1a_3 + a_2a_3 - a_1a_2 - 2a_1a_2a_3.$$

In what follows, μ_j^x denotes the 2×2 x-Pauli matrix, and $\hat{1}$ denotes the 2×2 identity matrix. We use a transformation to map the variables that appears in a term from (C7) into a 2×2 diagonal matrix:

$$a_1 \mapsto \frac{1}{2}(\hat{1} + \mu_1^x), \quad a_2 \mapsto \frac{1}{2}(\hat{1} + \mu_2^x), \quad a_3 \mapsto \frac{1}{2}(\hat{1} - \mu_3^x). \tag{C8}$$

A product of variables is mapped to the Kronecker product of the diagonal matrices. It is understood that a variable which does not appear in a product is mapped to the identity. Our choice of ordering the indices of the subsystems is (3,2,1). More precisely for our cost function, we have the operator

$$\hat{C} = \frac{1}{4}(\mu_1^x - \mu_2^x + \mu_3^x - 2\mu_1^x\mu_2^x - 2\mu_1^x\mu_3^x + \mu_1^x\mu_2^x\mu_3^x) \tag{C9}$$

associated to the cost function $C(a_1, a_2, a_3)$. In our paper, we scale this operator and define the Hamiltonian

$$\hat{H}_{\text{SAT}} = \hbar\omega(\mu_1^x - \mu_2^x + \mu_3^x - 2\mu_1^x\mu_2^x - 2\mu_1^x\mu_3^x + \mu_1^x\mu_2^x\mu_3^x), \tag{C10}$$

where ω has units of angular frequency. Once we have the Hamiltonian, the solution of the 3SAT problem is encoded in the ground state $|G\rangle$. In order to obtain to the triplet (a_1, a_2, a_3) satisfying the 3 clauses discussed above, we just

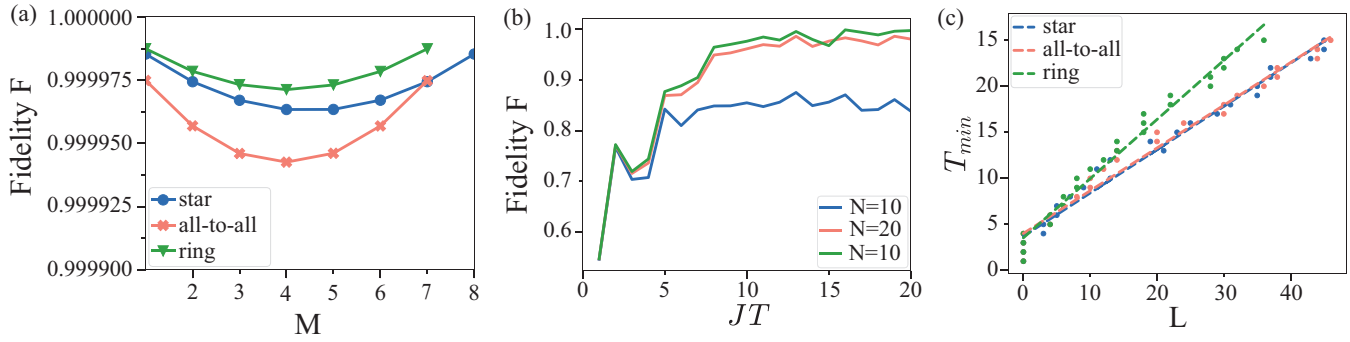

FIG. 7. (a) Fidelity $F = |\mathrm{tr}(\hat{\mathcal{F}}^{\dagger}_{\mathrm{target}}\hat{\mathcal{F}}_{\mathrm{trial}})|/D$ (D is the dimension of the Hilbert space) of effective dynamics for hard-core bosons in a driven chain and minimal time T_{min} to generate effective Hamiltonian with fidelity $F > 0.999$. All parameters are scaled in units of the nearest-neighbor coupling strength J. (a) Fidelity for star graph ($L = 9$ sites), all-to-all coupling ($L = 8$ sites), and ring ($L = 8$) sites. Driving with $N = 10$ timesteps and time $T = 10/J$, with driving of local potential in range $-5J < g_l < 5J$. (b) Fidelity of effective dynamics for driving time and timesteps of a linear chain with a $N_{\mathrm{p}} = 2$ excitation and $U = 4J$. All parameters are scaled in units of the nearest-neighbor coupling strength J. Target Hamiltonian is all-to-all coupling with $L = 8$ sites with driving of both potential ($-5J < g_l < 5J$) and nearest-neighbor coupling $-J < J_l < J$. (c) Minimal time needed T_{min} to generate effective Hamiltonian with fidelity $F > 0.999$, for varying system size of chain L and a single excitation $M = 1$. The result is fitted with a linear equation $T_{\mathrm{min}} = aL + b$ (dashed lines). The found slope is $a_{\mathrm{star}} = 0.47/J$, $a_{\mathrm{all}} = 0.46/J$ and $a_{\mathrm{ring}} = 0.64/J$. All parameters are scaled in units of the nearest-neighbor coupling strength J. Driving of potential is bounded between $-5J < g_l < 5J$ and a single timestep of the driving protocol is fixed to $\tau = 1/J$.

need to calculate the following expectation values

$$
\begin{aligned}
a_1 &= \frac{1}{2}\langle G|\left[1+\frac{1}{2}\left(\sigma_1^x\sigma_5^x+\sigma_1^y\sigma_5^y+\sigma_2^x\sigma_6^x+\sigma_2^y\sigma_6^y+\sigma_3^x\sigma_7^x+\sigma_3^y\sigma_7^y+\sigma_4^x\sigma_8^x+\sigma_4^y\sigma_8^y\right)\right]|G\rangle\\
a_2 &= \frac{1}{2}\langle G|\left[1+\frac{1}{2}\left(\sigma_1^x\sigma_3^x+\sigma_1^y\sigma_3^y+\sigma_2^x\sigma_4^x+\sigma_2^y\sigma_4^y+\sigma_5^x\sigma_7^x+\sigma_5^y\sigma_7^y+\sigma_6^x\sigma_8^x+\sigma_6^y\sigma_8^y\right)\right]|G\rangle \qquad \text{(C11)}\\
a_3 &= \frac{1}{2}\langle G|\left[1-\frac{1}{2}\left(\sigma_1^x\sigma_2^x+\sigma_1^y\sigma_2^y+\sigma_3^x\sigma_4^x+\sigma_3^y\sigma_4^y+\sigma_5^x\sigma_6^x+\sigma_5^y\sigma_6^y+\sigma_7^x\sigma_8^x+\sigma_7^y\sigma_8^y\right)\right]|G\rangle,
\end{aligned}
$$

which correspond to two-point correlations in the original basis of qubits [see Eq. (B1)].

2. Instantaneous Hamiltonian and driving protocols for the adiabatic deformation of the 3SAT Hamiltonian

In this section we provide additional information on the adiabatic deformation of the 3SAT Hamiltonian equation (C10). With this aim, we consider a single excitation $M = 1$ in an array of $L = 8$ sites and the dimension of the Hilbert space is $D_{1,9} = 9$. As we discussed above, we consider the basis $|1_l\rangle = |0, 0, \ldots, 1_l, 0, \ldots, 0\rangle$ with $l = 1, \ldots, L$, where $|1_l\rangle$ denotes an excitation at the lth site. In this case, we are not only able to simulate the target Hamiltonian, but we also perform an adiabatic modulation of the parameters to interpolate two effective Hamiltonians. The adiabatic evolution happens over 200 cycles, makes a total time of $T_{\mathrm{total}} = 1276/J$.

APPENDIX D: PERFORMANCE OF OUR METHOD AND ITS DEPENDENCE ON DIFFERENT PARAMETERS

In our paper, we present minimal examples of the applicability of our method. We were able to simulate such as star, all-to-all and ring connectivities and consider the case of interacting and Hardcore bosons as well. However, one might ask what is the scalability of method and what is its dependence on other parameters such as the number of steps in the driving protocol. This is precisely the goal of this section. First we discuss the scaling of the effective Hamiltonian with the number M of excitations in the hardcore boson regime. After that, we investigate scaling of the effective Hamiltonian in the case of two excitation with a finite interaction strength $U = 4J$ as a function of the period T and the number of steps N. Finally, we concentrate on the dependence of the effective Hamiltonian on the driving parameters.

1. Scaling of the method with respect to different parameters of the system

We discuss the case of many particles for the hard-core bosonic chain. Driving a hard-core chain generates arbitrary noninteracting fermionic many-body Hamiltonian. By using GRAPE, we calculate the best driving parameters for the single particle case first. Then, the same driving is used for the same system, but now with multiple excitations $M > 1$. The resulting effective Hamiltonian is then the corresponding fermionic many-body Hamiltonian. The scaling of the fidelity for star, all-to-all and ring connectivities is shown in Fig. 7(a).

As we discussed above, in the hardcore boson regime, one can solve the many-body problem just by obtaining the solution for a single particle, because effectively the system

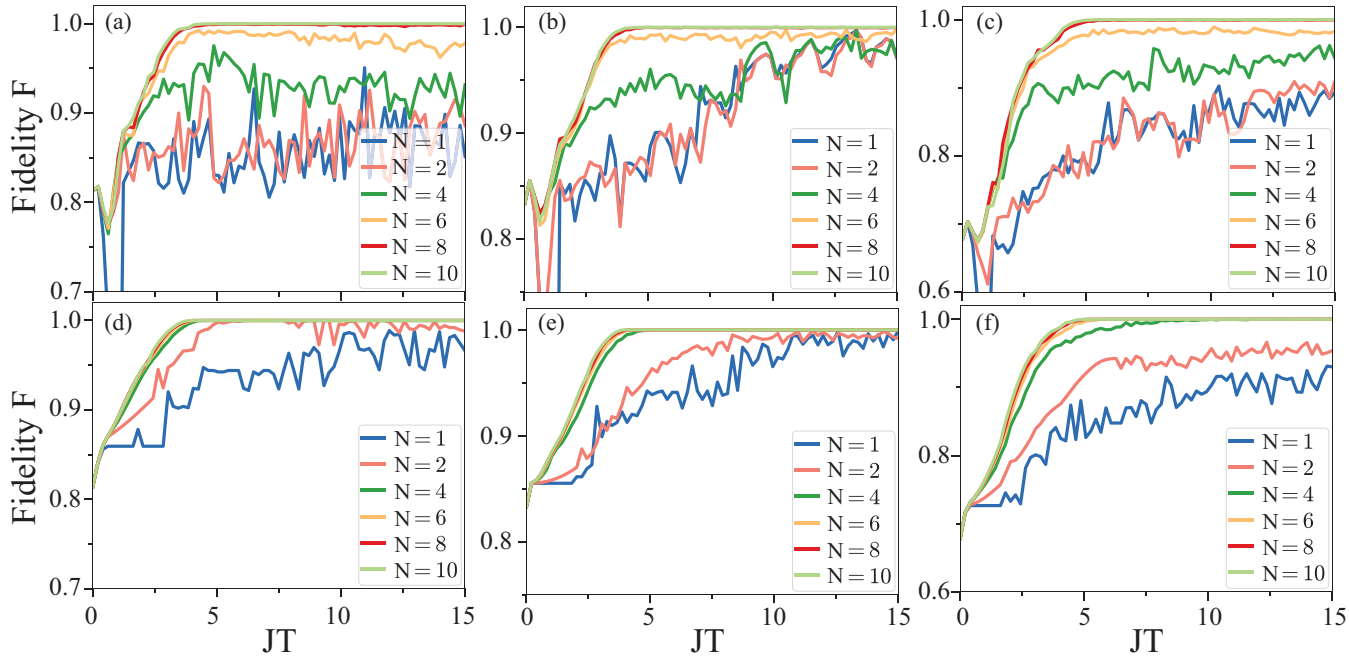

FIG. 8. Fidelity of effective dynamics for driving time and timesteps of a linear chain with a single excitation. All parameters are scaled in units of the nearest-neighbor coupling strength J. [(a),(d)] Target effective Hamiltonian is the star graph with $L = 9$ sites. [(b),(e)] Target is all-to-all coupling with $L = 8$ sites. [(c),(f)] Target is the simulation of boolean equations with $L = 8$ sites. [(a),(b),(c)] Driving of local potential only in range $-5J < g_l < 5J$. [(d),(e),(f)] Driving of both potential ($-5J < g_l < 5J$) and nearest-neighbor coupling $-J < J_l < J$.

is noninteracting and one can map it to a system of free fermions. However, for a finite value of the interaction $U = 4J$, the excitations are far from the hardcore boson regime, and we cannot reconstruct the solution to the two body problem by investigating the single particle case. For the Bose-Hubbard model with $M = 2$ particles, we note that more time steps N are needed to generate the effective Hamiltonian compared to the single particle case. To investigate this issue in detail, here we consider the case of a all-to-all connectivity and calculate the fidelity of the numerically obtained unitary operator with respect to target unitary. We explore the dependence of this fidelity as a function of the period T of the driving and the number of time steps, as we depict in Fig. 7(b).

We investigate the scaling of the effective Hamiltonian generation for varying system size. The result is shown in Fig. 7(c). We show the star-graph, all-to-all coupling and ring for single excitation and potential driving. We vary the system size L of the chain and calculate the minimal time needed $T_{\min}$ to generate the effective Hamiltonian for the given configuration with a fidelity $F > 0.999$. We fix the length of a time step of the driving protocol to $\tau = 1/J$, where J is the coupling strength of the chain. We observe an approximately linear scaling between protocol time $T_{\min}$ and system size L.

2. Effective Hamiltonian dependence on driving parameters

The fidelity of the effective Hamiltonian that can be generated depends on several parameters. We investigate here how the fidelity of the effective dynamics is affected by the driving time T as well as the number N of discrete steps of the driving protocol. The results for a driven linear chain are presented in Fig. 8. We generate a star graph [Figs. 8(a) and 8(d)], all-to-all coupling [Figs. 8(b) and 8(e)] and the boolean equations [Figs. 8(c) and 8(f)]. We use either driving of local potential only [Figs. 8(a), 8(b), and 8(c)] or drive both potential and nearest-neighbor couplings [Figs. 8(d), 8(e), and 8(f)]. We observe that when only the local potential is driven, at least $N = 8$ steps are needed to achieve sufficient fidelity. For driving both potential and nearest-neighbor coupling, 4 timesteps are sufficient. There is also a minimal time needed before maximal fidelity is reached, which is nearly the same for all three problems and on the order of $T_{\min} = 4/J$.

3. Robustness of the effective Hamiltonian against noise in the driving protocol

We investigate how noise in the driving parameters affects the fidelity of the effective dynamics. For that, we take the optimal driving protocol found without noise, and then perturb the driving parameters. We add to the optimal driving parameters an offset that is randomly sampled from the uniform distribution $\delta g_l \sim [-\delta/2, \delta/2]$ for every parameter and timestep independently. The result for the dataset of Fig. 2 in the main text are shown here in Fig. 9. We observe a decrease in the fidelity with increasing noise. Multi-excitations systems are affected more by noise (star 1 excitation, all-to-all 2 excitations and ring 3 excitations). We note that for all three systems, fidelity decreases by at most by 1% if random perturbation $\delta g < 0.1J$ or about 10% of the intra-chain couplings.

4. Scaling of computational effort

Our goal is to find the driving protocols that approximates the unitary that encodes the effective Hamiltonian. To do so,

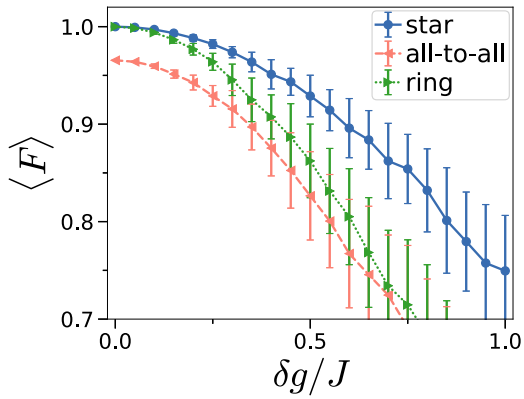

FIG. 9. Robustness of effective Hamiltonian to noise: Mean and standard deviation of fidelity of the effective dynamics for varying noise $\delta g_l(t)$ in the driving parameters $g(t)$. The driven on-site energies are perturbed by $g_l'(t_n) = g_l(t_n) + \text{uniform}\ (-\delta g/2, \delta g/2)$, which is sampled independently for all sites l and time step t_n, where uniform() is the uniform distribution. Fidelity is sampled over 100 random instances. Star, all-to-all and ring correspond to the same results in Fig. 2 of the main text. For all-to-all coupling, the time-dependent couplings are perturbed in a similar manner with a factor 5 less perturbation.

we need to do two things: Simulate the quantum system and find the parameters of the driving protocol. We simulate the dynamics of the quantum system on a classical computer. The simulation effort scales polynomially with the Hilbert space size, and quickly becomes not feasible for larger quantum systems. To find the driving protocol, we employ numerical methods such as GRAPE, as well as deep learning. The optimization problem can be difficult in general, as the optimization routine may become stuck in a local minima instead of the global minima. However, if the number of driving parameters is larger than the Hilbert space, the optimization problem is often characterized by many global minima and it is straightforward to solve it numerically [77,78].

APPENDIX E: FLOQUET SIMULATION OF LiH

In our paper we demonstrate the capability of our approach by simulating a LiH molecule at bond distance. The results of our simulation are shown in the in the main text. The corresponding parameters of the Hamiltonian can be found in [3]. They have been obtained by the STO-3G basis, where the atomic orbitals are approximated with three Gaussians to obtain one- and two-electron integrals for the electronic interactions [Slater-type orbital (STO)]. For the LiH molecule, the 1s orbital of H and the 1s, 2s and $2p_x$ and $2p_z$ were assumed to be occupied. Furthermore, all other orbitals are assumed to be empty. By including the parity symmetries, the LiH molecule can be described effectively by 4 qubits with a Hilberts pace of dimension 16. The Hamiltonian contains 99 coupling terms expressed as a product of different Pauli operators. For convenience, below we include the explicit form of the corresponding Hamiltonian matrix for LiH molecule, as follows

$$\begin{pmatrix}
.00846 & -.33392 & .03370 & -.21996 & .33392 & -.08335 & .10560 & -.08001 & -.03370 & .10560 & -.18833 & .09292 & -.21996 & .08001 & -.09292 & .10347 \\
-.33392 & -.02541 & -.21713 & .07039 & -.08335 & .37960 & -.04784 & .09209 & .10560 & -.17922 & -.00038 & -.13611 & .08001 & -.26748 & .05141 & -.09746 \\
.03370 & -.21713 & -.00029 & -.34549 & .10560 & -.04784 & .35689 & -.09255 & -.18833 & -.00038 & -.10054 & .13207 & -.09292 & .05141 & -.25612 & .09590 \\
-.21996 & .07039 & -.34549 & -.03981 & -.08001 & .09209 & -.09255 & .33823 & .09292 & -.13611 & .13207 & -.05945 & .10347 & -.09746 & .09590 & -.19952 \\
.33392 & -.08335 & .10560 & -.08001 & -.02541 & -.37960 & .17922 & -.26748 & -.21713 & .04784 & .00038 & .05141 & -.07039 & .09209 & -.13611 & .09746 \\
-.08335 & .37960 & -.04784 & .09209 & -.37960 & .15372 & -.11896 & .14861 & .04784 & -.11896 & .11505 & -.03415 & .09209 & -.14861 & .03415 & -.12120 \\
.10560 & -.04784 & .35689 & -.09255 & .17922 & -.11896 & .07367 & -.42903 & .00038 & .11505 & -.17038 & .03095 & -.13611 & .03415 & -.11232 & .11348 \\
-.08001 & .09209 & -.09255 & .33823 & -.26748 & .14861 & -.42903 & -.04424 & .05141 & -.03415 & .03095 & -.19948 & .09746 & -.12120 & .11348 & -.06392 \\
-.03370 & .10560 & -.18833 & .09292 & -.21713 & .04784 & .00038 & .05141 & -.00029 & -.35689 & .10054 & -.25612 & .34549 & -.09255 & .13207 & -.09590 \\
.10560 & -.17922 & -.00038 & -.13611 & .04784 & -.11896 & .11505 & -.03415 & -.35689 & .07367 & -.17038 & .11232 & -.09255 & .42903 & -.03095 & .11348 \\
-.18833 & -.00038 & -.10054 & .13207 & .00038 & .11505 & -.17038 & .03095 & .10054 & -.17038 & .05177 & -.39058 & .13207 & -.03095 & .39058 & -.11241 \\
.09292 & -.13611 & .13207 & -.05945 & .05141 & -.03415 & .03095 & -.19948 & -.25612 & .11232 & -.39058 & -.04576 & -.09590 & .11348 & -.11241 & .34422 \\
-.21996 & .08001 & -.09292 & .10347 & -.07039 & .09209 & -.13611 & .09746 & .34549 & -.09255 & .13207 & -.09590 & -.03981 & -.33823 & .05945 & -.19952 \\
.08001 & -.26748 & .05141 & -.09746 & .09209 & -.14861 & .03415 & -.12120 & -.09255 & .42903 & -.03095 & .11348 & -.33823 & -.04424 & -.19948 & .06392 \\
-.09292 & .05141 & -.25612 & .09590 & -.13611 & .03415 & -.11232 & .11348 & .13207 & -.03095 & .39058 & -.11241 & .05945 & -.19948 & -.04576 & -.34422 \\
.10347 & -.09746 & .09590 & -.19952 & .09746 & -.12120 & .11348 & -.06392 & -.09590 & .11348 & -.11241 & .34422 & -.19952 & .06392 & -.34422 & -.05026
\end{pmatrix} \tag{E1}$$

[1] J. Preskill, Quantum computing in the NISQ era and beyond, Quantum **2**, 79 (2018).

[2] F. Arute, K. Arya, R. Babbush, D. Bacon, J. C. Bardin, R. Barends, R. Biswas, S. Boixo, F. G. Brandao, D. A. Buell *et al.*, Quantum supremacy using a programmable superconducting processor, Nature (London) **574**, 505 (2019).

[3] A. Kandala, A. Mezzacapo, K. Temme, M. Takita, M. Brink, J. M. Chow, and J. M. Gambetta, Hardware-efficient variational quantum eigensolver for small molecules and quantum magnets, Nature (London) **549**, 242 (2017).

[4] Z. Yan, Y.-R. Zhang, M. Gong, Y. Wu, Y. Zheng, S. Li, C. Wang, F. Liang, J. Lin, Y. Xu *et al.*, Strongly correlated quantum walks with a 12-qubit superconducting processor, Science **364**, 753 (2019).

[5] R. Babbush, N. Wiebe, J. McClean, J. McClain, H. Neven, and Garnet Kin-Lic Chan, Low-Depth Quantum Simulation of Materials, Phys. Rev. X **8**, 011044 (2018).

[6] I. M. Georgescu, S. Ashhab, and F. Nori, Quantum simulation, Rev. Mod. Phys. **86**, 153 (2014).

[7] D. Deutsch, Quantum theory, the Church–turing principle and the universal quantum computer, Proc. R. Soc. A **400**, 97 (1985).

[8] R. Blatt and C. F. Roos, Quantum simulations with trapped ions, Nat. Phys. **8**, 277 (2012).

[9] S. McArdle, S. Endo, A. Aspuru-Guzik, S. C. Benjamin, and X. Yuan, Quantum computational chemistry, Rev. Mod. Phys. **92**, 015003 (2020).

[10] S. J. Devitt, W. J. Munro, and K. Nemoto, Quantum error correction for beginners, Rep. Prog. Phys. **76**, 076001 (2013).

[11] K. Bharti, A. Cervera-Lierta, T. H. Kyaw, T. Haug, S. Alperin-Lea, A. Anand, M. Degroote, H. Heimonen, J. S. Kottmann, T. Menke *et al.*, Noisy intermediate-scale quantum (NISQ) algorithms, Rev. Mod. Phys. **94**, 015004 (2022).

[12] T. Albash and D. A. Lidar, Adiabatic quantum computation, Rev. Mod. Phys. **90**, 015002 (2018).

[13] R. Harris, M.W. Johnson, T. Lanting, A.J. Berkley, J. Johansson, P. Bunyk, E. Tolkacheva, E. Ladizinsky, N. Ladizinsky, T. Oh, F. Cioata, I. Perminov, P. Spear, C. Enderud, C. Rich, S. Uchaikin, M.C. Thom, E.M. Chapple, J. Wang, B. Wilson *et al.*, Experimental investigation of an eight-qubit unit cell in a superconducting optimization processor, Phys. Rev. B **82**, 024511 (2010).

[14] G. Quiroz, Robust quantum control for adiabatic quantum computation, Phys. Rev. A **99**, 062306 (2019).

[15] E. Urban, T. A. Johnson, T. Henage, L. Isenhower, D. Yavuz, T. Walker, and M. Saffman, Observation of Rydberg blockade between two atoms, Nat. Phys. **5**, 110 (2009).

[16] M. W. Johnson, M. H. Amin, S. Gildert, T. Lanting, F. Hamze, N. Dickson, R. Harris, A. J. Berkley, J. Johansson, P. Bunyk *et al.*, Quantum annealing with manufactured spins, Nature (London) **473**, 194 (2011).

[17] I. Bloch, Quantum coherence and entanglement with ultracold atoms in optical lattices, Nature (London) **453**, 1016 (2008).

[18] D. Aharonov, D. Gottesman, S. Irani, and J. Kempe, The power of quantum systems on a line, Commun. Math. Phys. **287**, 41 (2009).

[19] N. Chancellor, S. Zohren, and P. A. Warburton, Circuit design for multi-body interactions in superconducting quantum annealing systems with applications to a scalable architecture, npj Quantum Inf. **3**, 21 (2017).

[20] W. Lechner, P. Hauke, and P. Zoller, A quantum annealing architecture with all-to-all connectivity from local interactions, Sci. Adv. **1**, e1500838 (2015).

[21] X. Qiu, P. Zoller, and X. Li, Programmable Quantum Annealing Architectures with Ising Quantum Wires, PRX Quantum **1**, 020311 (2020).

[22] P. Roushan, C. Neill, J. Tangpanitanon, V. M. Bastidas, A. Megrant, R. Barends, Y. Chen, Z. Chen, B. Chiaro, A. Dunsworth *et al.*, Spectroscopic signatures of localization with interacting photons in superconducting qubits, Science **358**, 1175 (2017).

[23] R. Ma, B. Saxberg, C. Owens, N. Leung, Y. Lu, J. Simon, and D. I. Schuster, A dissipatively stabilized Mott insulator of photons, Nature (London) **566**, 51 (2019).

[24] Y. Ye, Z.Y. Ge, Y. Wu, S. Wang, M. Gong, Y.R. Zhang, Q. Zhu, R. Yang, S. Li, F. Liang, J. Lin, Y. Xu, C. Guo, L. Sun, C. Cheng, N. Ma, Z.Y. Meng, H. Deng, H. Rong *et al.*, Propagation and Localization of Collective Excitations on a 24-Qubit Superconducting Processor, Phys. Rev. Lett. **123**, 050502 (2019).

[25] B. P. Lanyon, C. Hempel, D. Nigg, M. Müller, R. Gerritsma, F. Zähringer, P. Schindler, J. T. Barreiro, M. Rambach, G. Kirchmair *et al.*, Universal digital quantum simulation with trapped ions, Science **334**, 57 (2011).

[26] J. Zhang, P. Hess, A. Kyprianidis, P. Becker, A. Lee, J. Smith, G. Pagano, I.-D. Potirniche, A. C. Potter, A. Vishwanath *et al.*, Observation of a discrete time crystal, Nature (London) **543**, 217 (2017).

[27] P. Roushan, C. Neill, A. Megrant, Y. Chen, R. Babbush, R. Barends, B. Campbell, Z. Chen, B. Chiaro, A. Dunsworth *et al.*, Chiral ground-state currents of interacting photons in a synthetic magnetic field, Nat. Phys. **13**, 146 (2017).

[28] B. Chiaro, C. Neill, A. Bohrdt, M. Filippone, F. Arute, K. Arya, R. Babbush, D. Bacon, J. Bardin, R. Barends *et al.*, Growth and preservation of entanglement in a many-body localized system, arXiv:1910.06024.

[29] C. Zha, V.M. Bastidas, M. Gong, Y. Wu, H. Rong, R. Yang, Y. Ye, S. Li, Q. Zhu, S. Wang, Y. Zhao, F. Liang, J. Lin, Y. Xu, C.Z. Peng, J. Schmiedmayer, K. Nemoto, H. Deng, W.J. Munro, X. Zhu, and J.W. Pan, Ergodic-Localized Junctions in a Periodically Driven Spin Chain, Phys. Rev. Lett. **125**, 170503 (2020).

[30] K. X. Wei, P. Peng, O. Shtanko, I. Marvian, S. Lloyd, C. Ramanathan, and P. Cappellaro, Emergent Prethermalization Signatures in Out-of-Time Ordered Correlations, Phys. Rev. Lett. **123**, 090605 (2019).

[31] A. Rubio-Abadal, M. Ippoliti, S. Hollerith, D. Wei, J. Rui, S. L. Sondhi, V. Khemani, C. Gross, and I. Bloch, Floquet Prethermalization in a Bose-Hubbard System, Phys. Rev. X **10**, 021044 (2020).

[32] V. M. Bastidas, B. Renoust, K. Nemoto, and W. J. Munro, Ergodic-localized junctions in periodically driven systems, Phys. Rev. B **98**, 224307 (2018).

[33] A. Eckardt, Colloquium: Atomic quantum gases in periodically driven optical lattices, Rev. Mod. Phys. **89**, 011004 (2017).

[34] S. Restrepo, J. Cerrillo, V. M. Bastidas, D. G. Angelakis, and T. Brandes, Driven Open Quantum Systems and Floquet Stroboscopic Dynamics, Phys. Rev. Lett. **117**, 250401 (2016).

[35] M. Bukov, L. D'Alessio, and A. Polkovnikov, Universal high-frequency behavior of periodically driven systems: From dynamical stabilization to Floquet engineering, Adv. Phys. **64**, 139 (2015).

[36] T. Oka and S. Kitamura, Floquet engineering of quantum materials, Annu. Rev. Condens. Matter Phys. **10**, 387 (2019).

[37] M. Sameti and M. J. Hartmann, Floquet engineering in superconducting circuits: From arbitrary spin-spin interactions to the Kitaev honeycomb model, Phys. Rev. A **99**, 012333 (2019).

[38] A. Kay, Perfect, efficient, state transfer and its application as a constructive tool, Int. J. Quantum Inform. **08**, 641 (2010).

[39] A. Kay and P. J. Pemberton-Ross, Computation on spin chains with limited access, Phys. Rev. A **81**, 010301(R) (2010).

[40] U. Haeberlen and J. S. Waugh, Coherent averaging effects in magnetic resonance, Phys. Rev. **175**, 453 (1968).

[41] J. Choi, H. Zhou, H. S. Knowles, R. Landig, S. Choi, and M. D. Lukin, Robust Dynamic Hamiltonian Engineering of Many-Body Spin Systems, Phys. Rev. X **10**, 031002 (2020).

[42] S. Geier, N. Thaicharoen, C. Hainaut, T. Franz, A. Salzinger, A. Tebben, D. Grimshandl, G. Zürn, and M. Weidemüller, Floquet Hamiltonian engineering of an isolated many-body spin system, Science **374**, 1149 (2021).

[43] L. D'Alessio and M. Rigol, Long-Time behavior of Isolated Periodically Driven Interacting Lattice Systems, Phys. Rev. X **4**, 041048 (2014).

[44] A. Martin, L. Lamata, E. Solano, and M. Sanz, Digital-analog quantum algorithm for the quantum fourier transform, Phys. Rev. Research **2**, 013012 (2020).

[45] A. Galicia, B. Ramon, E. Solano, and M. Sanz, Enhanced connectivity of quantum hardware with digital-analog control, Phys. Rev. Research **2**, 033103 (2020).
[46] A. Parra-Rodriguez, P. Lougovski, L. Lamata, E. Solano, and M. Sanz, Digital-analog quantum computation, Phys. Rev. A **101**, 022305 (2020).
[47] T. Gonzalez-Raya, R. Asensio-Perea, A. Martin, L. C. Céleri, M. Sanz, P. Lougovski, and E. F. Dumitrescu, Digital-Analog Quantum Simulations Using the Cross-Resonance Effect, PRX Quantum **2**, 020328 (2021).
[48] D. V. Babukhin, A. A. Zhukov, and W. V. Pogosov, Hybrid digital-analog simulation of many-body dynamics with superconducting qubits, Phys. Rev. A **101**, 052337 (2020).
[49] T. Onodera, E. Ng, and P. L. McMahon, A quantum annealer with fully programmable all-to-all coupling via Floquet engineering, npj Quantum Inf. **6**, 48 (2020).
[50] N. K. Lysne, K. W. Kuper, P. M. Poggi, I. H. Deutsch, and P. S. Jessen, Small, Highly Accurate Quantum Processor for Intermediate-Depth Quantum Simulations, Phys. Rev. Lett. **124**, 230501 (2020).
[51] Z. Tosner, S. J. Glaser, N. Khaneja, and N. C. Nielsen, Effective Hamiltonians by optimal control: Solid-state nmr double-quantum planar and isotropic dipolar recoupling, J. Chem. Phys. **125**, 184502 (2006).
[52] J. Zhang, T.-C. Wei, and R. Laflamme, Experimental Quantum Simulation of Entanglement in Many-Body Systems, Phys. Rev. Lett. **107**, 010501 (2011).
[53] K. Kobzar, S. Ehni, T. E. Skinner, S. J. Glaser, and B. Luy, Exploring the limits of broadband 90 and 180 universal rotation pulses, J. Magn. Reson. **225**, 142 (2012).
[54] K. R. K. Rao, T. S. Mahesh, and A. Kumar, Efficient simulation of unitary operators by combining two numerical algorithms: An NMR simulation of the mirror-inversion propagator of an *xy* spin chain, Phys. Rev. A **90**, 012306 (2014).
[55] J. J. Sørensen, J. S. Nyemann, F. Motzoi, J. Sherson, and T. Vosegaard, Optimization of pulses with low bandwidth for improved excitation of multiple-quantum coherences in NMR of quadrupolar nuclei, J. Chem. Phys. **152**, 054104 (2020).
[56] D. Lu, K. Li, J. Li, H. Katiyar, A. J. Park, G. Feng, T. Xin, H. Li, G. Long, A. Brodutch *et al.*, Enhancing quantum control by bootstrapping a quantum processor of 12 qubits, npj Quantum Inf. **3**, 45 (2017).
[57] M. P. Estarellas, T. Osada, V. M. Bastidas, B. Renoust, K. Sanaka, W. J. Munro, and K. Nemoto, Simulating complex quantum networks with time crystals, Sci. Adv. **6**, eaay8892 (2020).
[58] V. M. Bastidas, M. P. Estarellas, T. Osada, K. Nemoto, and W. J. Munro, Quantum metamorphism, Phys. Rev. B **102**, 224307 (2020).
[59] T. Hensgens, T. Fujita, L. Janssen, X. Li, C. Van Diepen, C. Reichl, W. Wegscheider, S. D. Sarma, and L. M. Vandersypen, Quantum simulation of a Fermi–Hubbard model using a semiconductor quantum dot array, Nature (London) **548**, 70 (2017).
[60] B. E. Kane, A silicon-based nuclear spin quantum computer, Nature (London) **393**, 133 (1998).
[61] H. Zhang, K. Arai, C. Belthangady, J.-C. Jaskula, and R. L. Walsworth, Selective addressing of solid-state spins at the nanoscale via magnetic resonance frequency encoding, npj Quantum Inf. **3**, 31 (2017).
[62] S. Aaronson and A. Arkhipov, The computational complexity of linear optics, in *Proceedings of the forty-third annual ACM symposium on Theory of computing* (2011), pp. 333–342.
[63] H.-S. Zhong, H. Wang, Y.-H. Deng, M.-C. Chen, L.-C. Peng, Y.-H. Luo, J. Qin, D. Wu, X. Ding, Y. Hu *et al.*, Quantum computational advantage using photons, Science **370**, 1460 (2020).
[64] S. Lloyd and S. L. Braunstein, Quantum Computation Over Continuous Variables, Phys. Rev. Lett. **82**, 1784 (1999).
[65] S. Machnes, U. Sander, S. J. Glaser, P. de Fouquières, A. Gruslys, S. Schirmer, and T. Schulte-Herbrüggen, Comparing, optimizing, and benchmarking quantum-control algorithms in a unifying programming framework, Phys. Rev. A **84**, 022305 (2011).
[66] J. R. Johansson, P. D. Nation, and F. Nori, Qutip 2: A python framework for the dynamics of open quantum systems, Comput. Phys. Commun. **184**, 1234 (2013).
[67] R.-B. Wu, H. Ding, D. Dong, and X. Wang, Learning robust and high-precision quantum controls, Phys. Rev. A **99**, 042327 (2019).
[68] J. R. McClean, S. Boixo, V. N. Smelyanskiy, R. Babbush, and H. Neven, Barren plateaus in quantum neural network training landscapes, Nat. Commun. **9**, 4812 (2018).
[69] For the interested reader, our numerical code is available on Github, https://github.com/txhaug/quantum-driving.
[70] D. A. Battaglia, G. E. Santoro, and E. Tosatti, Optimization by quantum annealing: Lessons from hard satisfiability problems, Phys. Rev. E **71**, 066707 (2005).
[71] G. L. Mullen and D. Panario, *Handbook of Finite Fields* (CRC Press, Boca Raton, 2013).
[72] A. Tanaka and K. Nemoto, Adiabatic quantum computation along quasienergies, Phys. Rev. A **81**, 022320 (2010).
[73] E. Farhi, J. Goldstone, and S. Gutmann, Quantum adiabatic evolution algorithms with different paths, arXiv:quant-ph/0208135.
[74] Y. Susa, Y. Yamashiro, M. Yamamoto, and H. Nishimori, Exponential speedup of quantum annealing by inhomogeneous driving of the transverse field, J. Phys. Soc. J. **87**, 023002 (2018).
[75] N. Nagaosa, *Quantum Field Theory in Strongly Correlated Electronic Systems* (Springer Science & Business Media, Berlin, 1999).
[76] C. Gravel, D. Panario, and D. Thomson, Unicyclic strong permutations, Cryptography and Communications **11**, 1211 (2019).
[77] M. Bukov, Reinforcement learning for autonomous preparation of floquet-engineered states: Inverting the quantum Kapitza oscillator, Phys. Rev. B **98**, 224305 (2018).
[78] H. A. Rabitz, M. M. Hsieh, and C. M. Rosenthal, Quantum optimally controlled transition landscapes, Science **303**, 1998 (2004).